Electronic Supplementary Material

Model Structures of Inactive and Peptide Agonist Bound C5aR: Insight into Agonist Binding, Selectivity and Activation

Soumendra Rana* and Amita Rani Sahoo

Chemical Biology Laboratory, School of Basic Sciences, Indian Institute of Technology Bhubaneswar, Odisha 751007, India. Email: soumendra@iitbbs.ac.in

Tables S1 to S12, and Figures S1 to S21 are respectively provided.

Table S1. Summary of the structural analysis of 14 inactive and 6 active GPCRs. Rhodopsin is highlighted in bold.

Inactive GPCRs (PDB)	**Hepta-helical Topology**	**N and C-Terminus**	**8th Helix**	**2° str. in ECL2**	**2° str. in other loops**
Rho (1F88)	**Yes**	**M1-A348**	**Yes**	**Yes**	No
CXCR4 (3ODU)	Yes	P27-G328	Yes	Yes	No
CXCR1 (2LNL)	Yes	P29-G324	Yes	Yes	No
β_2AR (2RH1)	Yes	D29-L342	Yes	Yes	No
PAR1 (3VW7)	Yes	D91-C378	No	Yes	No
S_1P_1 (3V2W)	Yes	S17-I325	Yes	Yes	No
M_3R (4DAJ)	Yes	I64-T556	Yes	Yes	Partially ordered ICL2
M_2R (3UON)	Yes	T20-M456	Yes	Yes	Partially ordered ICL2
A_2A (3REY)	Yes	S7-S305	Yes		Partially ordered ICL2
Histamine H_1 (3RZE)	Yes	M28-I485	Yes		No
δ-Opioid (4EJ4)	Yes	R41-C328	Yes	Yes	Partially ordered ICL2
μ-Opioid (4DKL)	Yes	M65-I352	Yes	Yes	Partially ordered ICL2
CCR5 (4MBS)	Yes	P19-Q313	Yes	Yes	Partially ordered ICL2
Dopamine D_3 (3PBL)	Yes	Y32-C400	Yes	Yes	Partially ordered ICL2
Active GPCRs (PDB ID)					
Opsin (3DQB)	Yes	M1-N326	Yes	Yes	No
β_2AR (3P0G)	Yes	D23-R344	Yes	Yes	Partially ordered ICL2
A_2A (3QAK)	Yes	I3-L308	Yes		No
M_2R (4MQS)	Yes	K19-M456	Yes	Yes	Partially ordered ICL2
P_2Y_{12} (4PXZ)	Yes	S15-S305	Yes		No
FFAR1 (4PHU)	Yes	M1-G280	No	Yes	No

Table S2. Comparison of (%) sequence identity/similarity of C5aR with inactive GPCRs. Receptors highlighted in bold shares highest sequence identity and similarity with C5aR. Sequence alignment performed in ClustalX.

GPCRs (PDB)	(%) Sequence identity / similarity with C5aR
μ-Opioid (4DKL)	**27/53.4**
CXCR1 (2LNL)	**27.4/52**
CXCR4 (3ODU)	**24.5/50**
A_2A (3REY)	15.7/36
PAR1 (3VW7)	25/44
M_3R (4DAJ)	22/48
M_2R (3UON)	19/43
δ-Opioid (4EJ4)	25/48.8
Rho (1F88)	20.57/44
β_2AR (2RH1)	20.8/44
Histamine (3RZE)	17.7/42
S_1P_1 (3V2W)	15.7/43
CCR5 (4MBS)	21.7/52
D_3R (3PBL)	20.5/40.8

Table S3. Summary of the (%) sequence identity/similarity of each TM of C5aR with 7 helices of 14 inactive GPCRs. The top two helices recruited as templates in MODELLER for modelling the individual TMs of C5aR are listed. CXCR1 helices that share a good sequence similarity with 5 of the 7 TMs in C5aR are highlighted in bold. Sequence alignment performed in ClustalX.

C5aR TMs with highest (%) sequence identity / similarity							
GPCRs (PDB)	**TM1**	**TM2**	**TM3**	**TM4**	**TM5**	**TM6**	**TM7**
Rho (1F88)		Helix1 44/55				Helix6 40/76	
CXCR4 (3ODU)				Helix4 48/60	Helix6 36/56	Helix6 40/64	
CXCR1 (2LNL)	**Helix6 40/56**	**Helix2 44/72**	**Helix3 43/65**	**Helix1 36/60**	**Helix7 46/53**		
β_2AR (2RH1)							
PAR1 (3VW7)			Helix3 50/68				Helix7 37/50
S_1P_1 (3V2W)							
M_3R (4DAJ)							
M_2R (3UON)							
A_2A (3REY)							
Histamine H_1 (3RZE)							
δ-Opioid (4EJ4)	Helix1 40/63						
μ-Opioid (4DKL)							Helix5 34/50
CCR5 (4MBS)							
Dopamine D_3 (3PBL)							

Table S4. Sequence comparison of C5aR-ECL2 with β-hairpin motifs of ECL2 observed in other GPCRs. Receptor highlighted in bold displays the highest similarity with the ECL2 of C5aR.

ECL2 of GPCRs (PDB)	**(%) Sequence identity / similarity with ECL2 of C5aR**
Rho (1F88)	**28/48**
CXCR1 (2LNL)	20/40
CXCR4 (3ODU)	20/36
PAR1 (3VW7)	12/24
δ-Opioid (4EJ4)	16/32
μ-Opioid (4DKL)	16/32
CCR5 (4MBS)	12/32
FFAR1 (4PHU)	8/28

Table S5. Structural comparison of C5aR with other native and ICL3 engineered inactive GPCRs. Highest and lowest RMSD values between the native inactive GPCRs in a row are respectively, highlighted in bold and bold italics. Highest and lowest RMSD values displayed between the ICL3 engineered inactive GPCRs are underlined in bold. Backbone RMSD calculation done in the absence of protein engineered into the ICL3.

GPCRs*	Rho	CXCR1	CXCR4	A_2A	PAR1	M_3R	M_2R	δ-Opioid	μ-Opioid	β_2AR	H_1R	S_1P_1	CCR5	D_3R	C5aR
Rho	0	**5.837**	2.637	1.979	3.933	2.825	2.436	2.792	1.874	2.141	2.282	3.508	***1.820***	1.829	5.440
CXCR1	***5.837***	0	6.555	7.510	7.228	6.075	6.200	6.920	6.428	6.380	5.815	**7.965**	6.669	6.784	5.346
CXCR4	2.637	6.555	0	2.973	3.767	4.172	2.13	1.820	**1.543**	2.487	3.122	**5.077**	1.863	2.15	6.056
A_2A	1.979	7.510	2.973	0	**4.421**	1.591	1.676	2.302	1.759	**1.280**	1.371	1.281	2.902	2.532	6.541
PAR1	3.933	7.228	3.767	**4.421**	0	3.333	3.711	2.491	2.558	2.759	**2.323**	4.172	2.472	3.454	6.146
M_3R	2.825	6.075	**4.172**	1.591	3.333	0	**0.616**	1.627	1.766	1.345	1.169	2.168	1.927	1.393	4.999
M_2R	2.436	6.200	2.13	1.676	**3.711**	**0.616**	0	1.638	1.684	1.197	1.210	2.293	2.231	1.294	5.487
δ-Opioid	2.792	6.920	1.820	2.302	2.491	1.627	1.638	0	**0.638**	1.399	1.208	**3.073**	1.441	2.903	5.402
μ-Opioid	1.874	6.428	1.543	1.759	**2.558**	1.766	1.684	**0.638**	0	1.426	1.200	2.466	1.429	1.432	5.183
β_2AR	2.141	6.380	2.487	1.280	**2.759**	1.188	1.197	1.399	1.426	0	1.126	1.298	1.507	**0.872**	5.740
H_1R	2.282	5.815	**3.122**	1.371	2.323	**1.068**	1.210	1.208	1.200	1.126	0	1.536	1.368	1.139	4.986
S_1P_1	3.508	7.965	**5.077**	**1.281**	4.172	2.046	2.293	3.073	2.466	1.298	1.536	0	3.325	1.629	6.183
CCR5	1.820	6.669	1.863	2.902	2.472	1.927	2.231	1.441	1.429	1.507	**1.368**	**3.325**	0	2.744	4.639
D_3R	1.829	6.784	2.150	2.532	**3.454**	1.393	1.294	2.903	1.432	**0.872**	1.139	1.629	2.744	0	5.706
C5aR	5.440	5.346	6.056	**6.541**	6.146	4.999	5.487	5.402	5.183	5.740	4.986	6.183	***4.639***	5.706	0

* **Rho**: 1F88; **β_2AR**: 2RH1; **A_2A**: 3REY; **M_2R**: 3UON; **CXCR1**: 2LNL; **CXCR4**: 3ODU; **PAR1**: 3VW7; **M_3R**: 4DAJ; **δ-Opioid**: 4EJ4; **μ-Opioid**: 4DKL; **Histamine H1**: 3RZE; **S_1P_1**: 3V2W; **CCR5**: 4MBS; **D_3R**: 3PBL

Table S6. Comparison of interhelical angles (Θ ± SD) between the helix axes of 14 inactive and 6 active GPCRs, as listed in Table S1. Θ values are calculated in MoLMoL and are highlighted in bold for the active GPCRs.

TMs	Helix1	Helix2	Helix3	Helix4	Helix5	Helix6	Helix7
Helix1	0	157.4 ± 5.2	44.2 ± 6.8	152.1 ± 6.8	44.9 ± 4.4	149 ± 7.8	26.9 ± 5.7
		158.6 ± 4	**45.7 ± 2**	**152 ± 4.2**	**50.4 ± 4.8**	**139.7 ± 6.5**	**23 ± 5.8**
Helix2	157.4 ± 5.2	0	155.3 ± 5.8	26.4 ± 5.7	147.5 ± 6.9	34.7 ± 4.4	147.4 ± 4
	158.6 ± 4		**153.5 ± 3.2**	**23.7 ± 4**	**141.3 ± 6.1**	**36 ± 7.9**	**149 ± 7**
Helix3	44.2 ± 6.8	155.3 ± 5.8	0	148.1 ± 3.4	20.7 ± 5.1	140.3 ± 7.2	41.2 ± 8.4
	45.7 ± 2	**153.5 ± 3.2**		**151.4 ± 2.7**	**21.7 ± 4.2**	**148 ± 6.3**	**42 ± 3.6**
Helix4	152.1 ± 6.8	26.4 ± 5.7	148.1 ± 3.4	0	157.9 ± 7.2	13.4 ± 4.2	165.7 ± 6.8
	152 ± 4.2	**23.7 ± 4**	**151.4 ± 2.7**		**155.9 ± 5**	**15.5 ± 5.8**	**165 ± 5.1**
Helix5	44.9 ± 4.4	147.5 ± 6.9	20.7 ± 5.1	157.9 ± 7.2	0	154.5 ± 3.3	28.8 ± 7.4
	50.4 ± 4.8	**141.3 ± 6.1**	**21.7 ± 4.2**	**155.9 ± 5**		**163 ± 6.4**	**35.5 ± 5.6**
Helix6	149 ± 7.8	34.7 ± 4.4	140.3 ± 7.2	13.4 ± 4.2	154.5 ± 3.3	0	170.3 ± 5.6
	139.7 ± 6.5	**36 ± 7.9**	**148 ± 6.3**	**15.5 ± 5.8**	**163 ± 6.4**		**159.6 ± 5.4**
Helix7	26.9 ± 5.7	147.4 ± 4	41.2 ± 8.4	165.7 ± 6.8	28.8 ± 7.4	170.3 ± 5.6	0
	23 ± 5.8	**149 ± 7**	**42 ± 3.6**	**165 ± 5.1**	**35.5 ± 5.6**	**159.6 ± 5.4**	

Table S7. Comparison of interhelical angles (Θ ± SD) calculated for the C5aR structures against the interhelical angles calculated across the 14 inactive GPCRs (Table S1). Θ values are calculated in MoLMoL. Closely matching Θ values are highlighted in bold.

TMs	**TM1**	**TM2**	**TM3**	**TM4**	**TM5**	**TM6**	**TM7**
TM1	0	157.4 ± 5.2[a], 147.8 ± 2.8[b], (149.4)	44.2 ± 6.8[a], 20.8 ± 1.1[b], (25.3)	152.1 ± 6.8[a], **152.6 ± 1.8[b], (150.7)**	44.9 ± 4.4[a], **42.4 ± 1.8[b], (43.1)**	149 ± 7.8[a], **153.2 ± 2.2[b], (159.7)**	26.9 ± 5.7[a], **28.1 ±.1.16[b], (29.0)**
TM2	157.4 ± 5.2[a], 147.8 ± 2.8[b], (149.4)	0	155.3 ± 5.8[a], 166.2 ± 2.09[b], (168.7)	26.4 ± 5.7[a], 43.31 ± 2.0[b], (43.6)	147.5 ± 6.9[a], **144.1 ± 1.01[b], (144.4)**	34.7 ± 4.4[a], **39.01 ± 1.36[b], (30.5)**	147.4 ± 4[a], **144.7 ± 0.85[b], (144.7)**
TM3	44.2 ± 6.8[a], 20.8 ± 1.1[b], (25.3)	155.3 ± 5.8[a], 166.2 ± 2.09[b], (168.7)	0	148.1 ± 3.4[a], **149.7 ± 1.5[b], (147.5)**	20.7 ± 5.1[a], 29.5 ± 0.85[b], (26.5)	140.3 ± 7.2[a], 153.64 ± 1.5[b], (160.3)	41.2 ± 8.4[a], 23.52 ± 0.98[b], (24.0)
TM4	152.1 ± 6.8[a], **152.6 ± 1.8[b], (150.7)**	26.4 ± 5.7[a], 43.31 ± 2.0[b], (43.6)	148.1 ± 3.4[a], **149.7 ± 1.5[b], (147.5)**	0	157.9 ± 7.2[a], **154.48 ± 0.7[b], (154.1)**	13.4 ± 4.2[a], 5.09 ± 1.37[b], (13.3)	165.7 ± 6.8[a], **169.7 ± 1.98[b], (169.8)**
TM5	44.9 ± 4.4[a], **42.4 ± 1.8[b], (43.1)**	147.5 ± 6.9[a], **144.1 ± 1.01[b], (144.4)**	20.7 ± 5.1[a], 29.5 ± 0.85[b], (26.5)	157.9 ± 7.2[a], **154.48 ± 0.7[b], (154.1)**	0	154.5 ± 3.3[a], **158.55 ±1.21[b], (156.1)**	28.8 ± 7.4[a], 16.79 ± 2.23[b], (17.3)
TM6	149 ± 7.8[a], **153.2 ± 2.2[b], (159.7)**	34.7 ± 4.4[a], **39.01 ± 1.36[b], (30.5)**	140.3 ± 7.2[a], 153.64 ± 1.5[b], (160.3)	13.4 ± 4.2[a], 5.09 ± 1.37[b], (13.3)	154.5 ± 3.3[a], **158.55 ±1.21[b], (156.1)**	0	170.3 ± 5.6[a], **174.4 ± 1.39[b], (171.2)**
TM7	26.9 ± 5.7[a], **28.1 ±.1.16[b], (29.0)**	147.4 ± 4[a], **144.7 ± 0.85[b], (144.7)**	41.2 ± 8.4[a], 23.52 ± 0.98[b], (24.0)	165.7 ± 6.8[a], **169.7 ± 1.98[b], (169.8)**	28.8 ± 7.4[a], 16.79 ± 2.23[b], (17.3)	170.3 ± 5.6[a], **174.4 ± 1.39[b], (171.2)**	0

*a = Inactive GPCRs

b = Calculated for 10 C5aR conformers from cluster 1, representing the inactive state of C5aR (Θ for central structure of cluster 1)

Table S8. Comparison of interhelical angles (Θ) of the C5aR (underlined in bold) with the chemokine receptors CXCR1, CXCR4 and CCR5, revealing high level of similarity in topology. Θ values are calculated in MoLMoL.

TMs	TM1	TM2	TM3	TM4	TM5	TM6	TM7
TM1	0	**149.4[a]**	**25.3[a]**	**150.7[a]**	**43.1[a]**	**159.7[a]**	**29.0[a]**
		147.1[b]	27.5[b]	156.7[b]	36.7[b]	170.6[b]	30.1[b]
		151.3[c]	52.7[c]	147.5[c]	46.1[c]	152.6[c]	20.7[c]
		156.3[d]	46.5[d]	162.8[d]	38.5[d]	159.2[d]	22[d]
TM2	**149.4[a]**	0	**168.7[a]**	**43.6[a]**	**144.4[a]**	**30.5[a]**	**144.7[a]**
	147.1[b]		171[b]	44[b]	161.8[b]	30.6[b]	150.4[b]
	151.3[c]		154.2[c]	18.3[c]	151.2[c]	32.2[c]	141.5[c]
	156.3[d]		152.1[d]	24.2[d]	147[d]	32.6[d]	140.1[d]
TM3	**25.3[a]**	**168.7[a]**	0	**147.5[a]**	**26.5[a]**	**160.3[a]**	**24.0[a]**
	27.5[b]	171[b]		144.6[b]	12.8[b]	156.7[b]	20.9[b]
	52.7[c]	154.2[c]		155.8[c]	19.3[c]	137.6[c]	54.7[c]
	46.5[d]	152.1[d]		144.7[d]	22.4[d]	138.4[d]	51.5[d]
TM4	**150.7[a]**	**43.6[a]**	**147.5[a]**	0	**154.1[a]**	**13.3[a]**	**169.8[a]**
	156.7[b]	44[b]	144.6[b]		143.8[b]	16.5[b]	158.9[b]
	147.5[c]	18.3[c]	155.8[c]		166.3[c]	18.7[c]	149.5[c]
	162.8[d]	24.2[d]	144.7[d]		158.2[d]	8.5[d]	162.8[d]
TM5	**43.1[a]**	**144.4[a]**	**26.5[a]**	**154.1[a]**	0	**156.1[a]**	**17.3[a]**
	36.7[b]	161.8[b]	12.8[b]	143.8[b]		150.3[b]	16[b]
	46.1[c]	151.2[c]	19.3[c]	166.3[c]		153.4[c]	40.4[c]
	38.5[d]	147[d]	22.4[d]	158.2[d]		156[d]	33.4[d]
TM6	**159.7[a]**	**30.5[a]**	**160.3[a]**	**13.3[a]**	**156.1[a]**	0	**171.2[a]**
	170.6[b]	30.6[b]	156.7[b]	16.5[b]	150.3[b]		159[b]
	152.6[c]	32.2[c]	137.6[c]	18.7[c]	153.4[c]		165.9[c]
	159.2[d]	32.6[d]	138.4[d]	8.5[d]	156[d]		170.1[d]
TM7	**29.0[a]**	**144.7[a]**	**24.0[a]**	**169.8[a]**	**17.3[a]**	**171.2[a]**	0
	30.1[b]	150.4[b]	20.9[b]	158.9[b]	16[b]	159[b]	
	20.7[c]	141.5[c]	54.7[c]	149.5[c]	40.4[c]	165.9[c]	
	22[d]	140.1[d]	51.5[d]	162.8[d]	33.4[d]	170.1[d]	

*a = Inactive C5aR presented in Figure 1a; b = Inactive CXCR1 (PDB: 2LNL); c = Inactive CXCR4 (PDB: 3ODU); d = Inactive CCR5 (PDB: 4MBS)

Table S9. Summary of the pharmacological activity, observed for the linear decapeptide (YSFKPMPLaR) agonist in several signaling studies, as described in the literature.

Tissue Types	Assay Types	IC50 (μM)	EC50 (μM)
Human fetal artery	Histamine activity		0.2
Human PMNs	β-Glucuronidase activity		4.1
Human PMNs	Competitive Binding with [^{125}I] C5a	6	
Human PMNs	Myeloperoxidase Release and Competitive Binding with [^{125}I] C5a	4.73	5.33
RBL cells	Competitive Binding with [^{125}I] C5a	8	
RBL cells	5-Hydroxyl-[^{3}H] tryptamine activity		0.08
Human fetal artery	Histamine activity		6.48
Human umbilical artery	Histamine activity		0.01
Human PMNs	Myeloperoxidase activity		1.32
Human PMNs	Competitive Binding with [^{125}I] C5a	2.34	
Human umbilical artery	Histamine activity		0.22
Human PMNs	Myeloperoxidase activity		4.43
Human PMNs	Competitive Binding with [^{125}I] C5a	13	
Rat macrophage	Competitive Binding with [^{125}I] C5a	0.2	
Rat PMNs	Competitive Binding with [^{125}I] C5a	0.1	
Engineered Yeast	β-Galactosidase activity		0.005
Human PMNs	Competitive Binding with [^{125}I] C5a	1.18	

Table S10. Details of the intermolecular interactions observed respectively, for the peptide agonist and the mutant peptide with C5aR. The estimated Ki values obtained from AutoDock4.2 are also noted.

Ligands[a]	**Intermolecular Interactions**			**Binding Energy (kcal/mol)**	**K_i (μM)**
	H-bond interactions (Å)	**Cation-π interactions (Å)**	**Salt bridge interactions (Å)**		
Peptide agonist (Y_1SFKPMPLaR_{10})	Y1:HH–R34:O (2.06)	K4:NZ–F275 (4.25)	NH_3^+–E269:OE1 (3.13)	-7.59	2.75
	NH_3^+–E269:OE1 (2.40)		NH_3^+–E269:OE2 (2.96)		
	NH_3^+–E269:OE2 (2.03)		R10:NH1–D191:OD1 (2.97)		
	S2:HN–E269:OE1 (1.90)		R10:NH2–D191:OD2 (2.97)		
	S2:HG–T32:OG1 (1.69)				
	K4:HZ1–F275:O (1.82)				
	CO_2^-–K185:HZ3 (1.91)				
	R10:HH12–D191:OD1 (2.14)				
	R10:HH22–D191:OD2 (1.97)				
Mutant peptide (Y_1SF<u>k</u>PMPLaR_{10})	Y1:O–K185:HZ1 (2.07)	K185:NZ–F3 (3.96)	K4:NZ–E269:OE1 (3.16)	-0.38	5.3 X 10^5
	K4:HZ3–E269:OE1 (2.41)		R10:NH2–E269:OE2 (2.94)		
	R10:HH22–E269:OE2 (2.27)		R10:NH2–E269:OE1 (2.51)		

* a = D-Ala, <u>k</u> = D-Lys; $NH3^+$ and $CO2^-$ respectively represent the N and C-terminus of the peptide agonist. Y1, S2, K4, and R10 represent the interacting residues on the peptide. T32, R34, K185, D191, E269 and F275 represent the interacting residues on the C5aR.

Table S11. Summary of the comparative pharmacological activity observed for C5a and *des*-R74-C5a in different tissues described in the literature. Values shown in bold correspond to *des*-R74-C5a.

Tissue type	**Assay type**	**C5aR**			
		IC50 (nM)	**EC50 (nM)**	**ED50 (nM)**	**ID50 (nM)**
RBL cells	Competitive Binding with [^{125}I] C5a	19 **412**			
Human Monocytes	Glucosaminidase Activity			0.85 **1**	
CHO cells	Competitive Binding with [^{125}I] C5a		5.52 **527**		
RBL cells	Hexosaminidase Activity		5.82 **21.2**		
Human Lymphoblasts	Competitive Binding with [^{125}I] C5a	3.4 **660**			
RBL cells	N-acetyl-β-D-glucosaminidase Activity		1.05 **0.89**		
RBL cells	Competitive Binding with [^{125}I] C5a	20.5 **411**			
Human Neutrophils	Chemotactic Activity			1 **100**	1.3 **420**
Human Monocytes	Competitive Binding with [^{125}I] C5a				1.4 **250**
RBL cells	Competitive Binding with [^{125}I] C5a	14 **604**			

Table S12. Comparison of change in inter-helical angles ($\Delta\Theta = \Theta_{Inactive} - \Theta_{Active}$) calculated for inactive-to-meta-active transition in C5aR, against the other GPCR pairs. Significant changes ($\Delta\Theta \geq \pm 4°$) are highlighted in bold italics and the highest magnitudes of changes are underlined in bold. $\Delta\Theta$ for helix3-helix6 pairs are highlighted in grey box. Θ values are calculated in MoLMoL

TMs	Helix1	Helix2	Helix3	Helix4	Helix5	Helix6	Helix7
Helix1	0	0^{a} 1.4^{b} ***6.6*^{c}** 2^{d} ***4.2*^{e}**	-1.6^{a} 2.3^{b} ***-7.8*^{c}** -2.3^{d} 0.7^{e}	***-6.6*^{a}** 2.7^{b} -0.1^{c} 2.5^{d} -0.6^{e}	2.1^{a} -0.6^{b} ***-6.8*^{c}** ***-8.4*^{d}** -0.1^{e}	***6.8*^{a}** ***4.3*^{b}** ***9.8*^{c}** ***7.3*^{d}** ***6.8*^{e}**	***4.3*^{a}** ***10.2*^{b}** ***5.1*^{c}** ***7.2*^{d}** ***-5.2*^{e}**
Helix2	0^{a} 1.4^{b} ***6.6*^{c}** 2^{d} ***4.2*^{e}**	0	***5.9*^{a}** -3.6^{b} 1.9^{c} 0.7^{d} -0.3^{e}	-0.8^{a} 0.9^{b} 3.7^{c} 0.5^{d} 1.7^{e}	***5.8*^{a}** 0.3^{b} 1.7^{c} ***9.6*^{d}** ***-5.6*^{e}**	***-4.5*^{a}** 0.9^{b} -3.7^{c} 1.1^{d} -2.8^{e}	-0.3^{a} -0.2^{b} -3.2^{c} -3.8^{d} -3.1^{e}
Helix3	-1.6^{a} 2.3^{b} ***-7.8*^{c}** -2.3^{d} 0.7^{e}	***5.9*^{a}** -3.6^{b} 1.9^{c} 0.7^{d} -0.3^{e}	0	-0.4^{a} ***-6.2*^{b}** ***-4.2*^{c}** -2.4^{d} ***5.8*^{e}**	0.9^{a} -1.8^{b} ***5*^{c}** -2.1^{d} ***-8*^{e}**	***-7.9*^{a}** ***-8.5*^{b}** ***-9.4*^{c}** **-22.2^{d}** **11.1^{e}**	3.5^{a} ***-4.1*^{b}** 0.7^{c} 2.8^{d} ***-8.6*^{e}**
Helix4	***-6.6*^{a}** 2.7^{b} -0.1^{c} 2.5^{d} -0.6^{e}	-0.8^{a} 0.9^{b} 3.7^{c} 0.5^{d} 1.7^{e}	-0.4^{a} ***-6.2*^{b}** ***-4.2*^{c}** -2.4^{d} **5.8^{e}**	0	3.2^{a} ***-4.7*^{b}** 3.4^{c} ***4.4*^{d}** 0.2^{e}	-3.5^{a} -2^{b} ***-8.8*^{c}** 3.2^{d} ***4.4*^{e}**	***-4*^{a}** ***10.6*^{b}** 3.3^{c} 1.8^{d} ***4.5*^{e}**
Helix5	2.1^{a} -0.6^{b} ***-6.8*^{c}** ***-8.4*^{d}** -0.1^{e}	***5.8*^{a}** 0.3^{b} 1.7^{c} ***9.6*^{d}** ***-5.6*^{e}**	0.9^{a} -1.8^{b} ***5*^{c}** -2.1^{d} ***-8*^{e}**	3.2^{a} ***-4.7*^{b}** 3.4^{c} ***4.4*^{d}** 0.2^{e}	0	**-13.5^{a}** ***-8.1*^{b}** ***7.7*^{c}** ***-21.9*^{d}** ***-4.5*^{e}**	3.2^{a} ***-9.1*^{b}** ***-7.4*^{c}** ***-6.6*^{d}** ***5.8*^{e}**
Helix6	***6.8*^{a}** ***4.3*^{b}** ***9.8*^{c}** ***7.3*^{d}** ***6.8*^{e}**	***-4.5*^{a}** 0.9^{b} -3.7^{c} 1.1^{d} -2.8^{e}	***-7.9*^{a}** ***-8.5*^{b}** ***-9.4*^{c}** **-22.2^{d}** **11.1^{e}**	-3.5^{a} -2^{b} ***-8.8*^{c}** 3.2^{d} ***4.4*^{e}**	**-13.5^{a}** ***-8.1*^{b}** ***7.7*^{c}** ***-21.9*^{d}** ***-4.5*^{e}**	0	***10.8*^{a}** **16.7^{b}** **17.2^{c}** ***15.5*^{d}** -0.7^{e}
Helix7	***4.3*^{a}** ***10.2*^{b}** ***5.1*^{c}** ***7.2*^{d}** ***-5.2*^{e}**	-0.3^{a} -0.2^{b} -3.2^{c} -3.8^{d} -3.1^{e}	3.5^{a} ***-4.1*^{b}** 0.7^{c} 2.8^{d} ***-8.6*^{e}**	***-4*^{a}** ***10.6*^{b}** 3.3^{c} 1.8^{d} ***4.5*^{e}**	3.2^{a} ***-9.1*^{b}** ***-7.4*^{c}** ***-6.6*^{d}** ***5.8*^{e}**	***10.8*^{a}** **16.7^{b}** **17.2^{c}** ***15.5*^{d}** -0.7^{e}	0

*a = Rhodopsin (1F88: Inactive; 3DQB: Active); b = A_2A (3REY: Inactive; 3QAK: Active); c = β_2AR (2RH1: Inactive; 3P0G: Active); d = M_2R (3UON: Inactive; 4MQS: Active); e = C5aR (Figure 1a: Inactive; Energy minimized Figure 2a: Active)

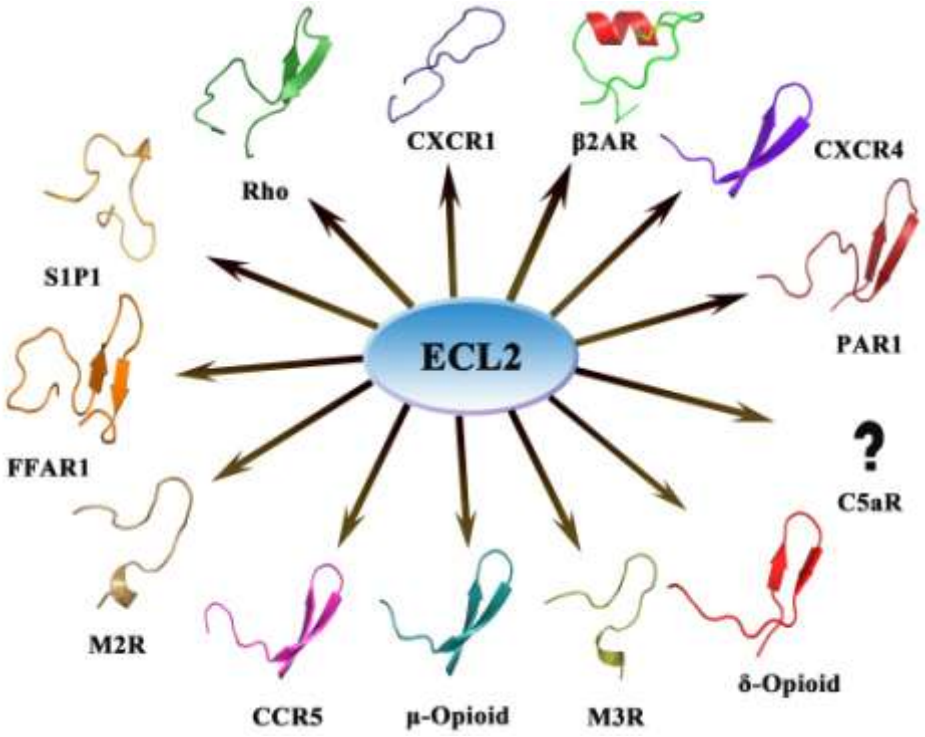

Fig. S1. The structural diversity of ECL2 observed across the inactive and active GPCRs. ECL2s displaying no structural changes in active states are not presented. ECL2s not resolved properly in GPCRs are also not shown.

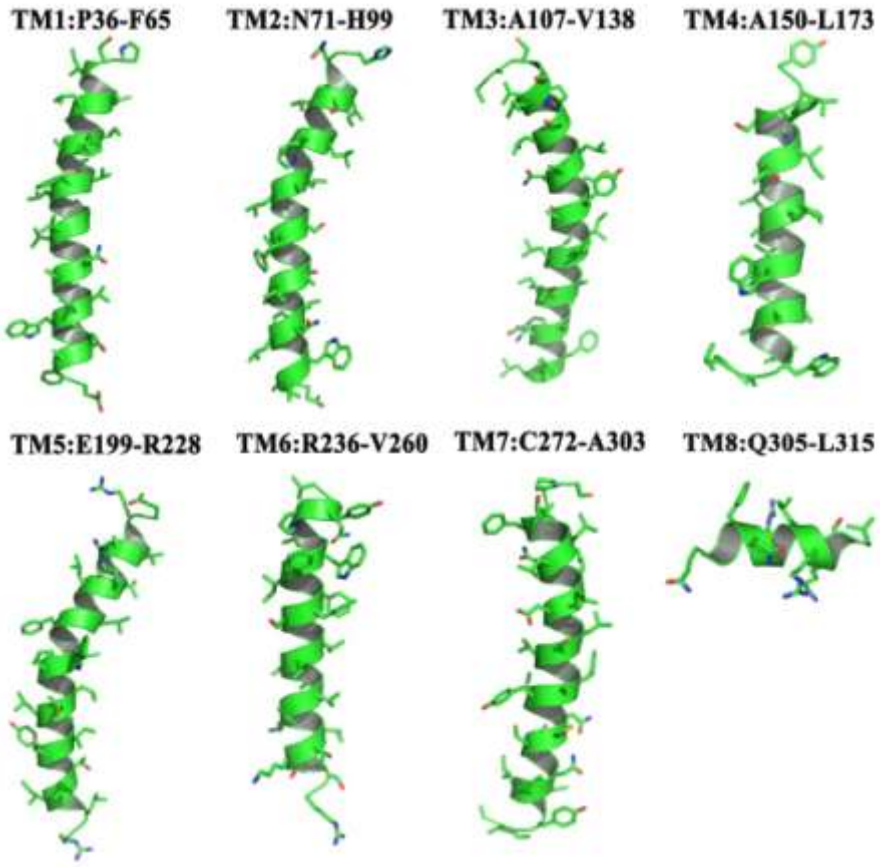

Fig. S2. Model structures of the C5aR TMs (1-7) obtained by implementing the multi template approach in MODELLER. The templates were selected from a matrix of 7 X 14 helices of inactive GPCRs. The 8th TM was modelled based on the CXCR1 template.

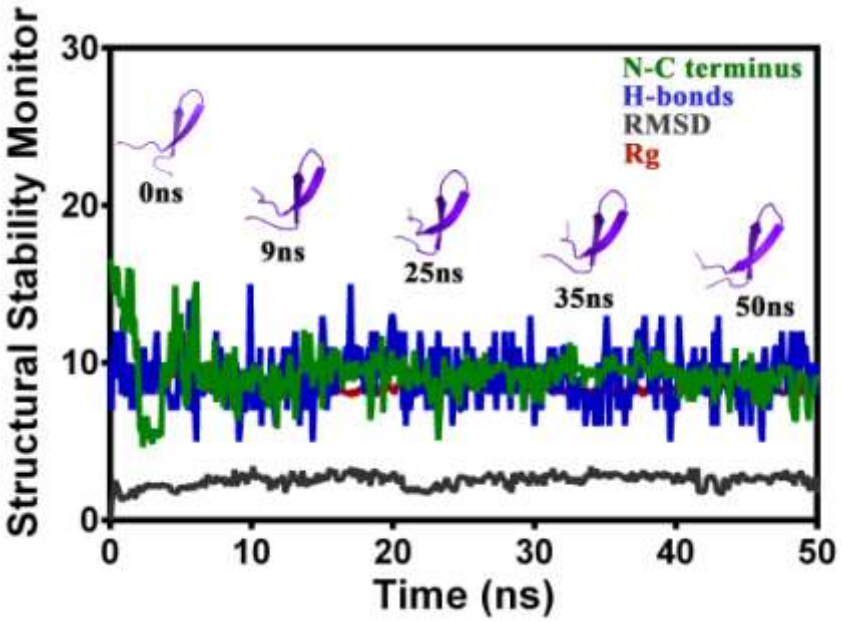

Fig. S3. Monitoring the structural stability of the ECL2 β-hairpin structure observed in CXCR4 receptor, sans the connecting helices over 50 ns of MD in explicit water at 300K.

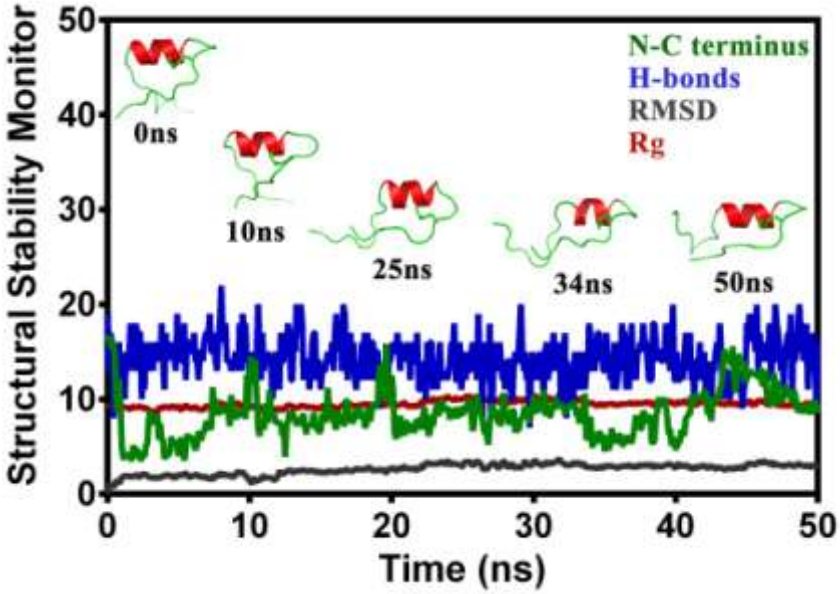

Fig. S4. Monitoring the structural stability of the loop-helix-loop structure of the ECL2 observed in β2AR receptor sans the connecting helices, over 50 ns of MD in explicit water at 300K.

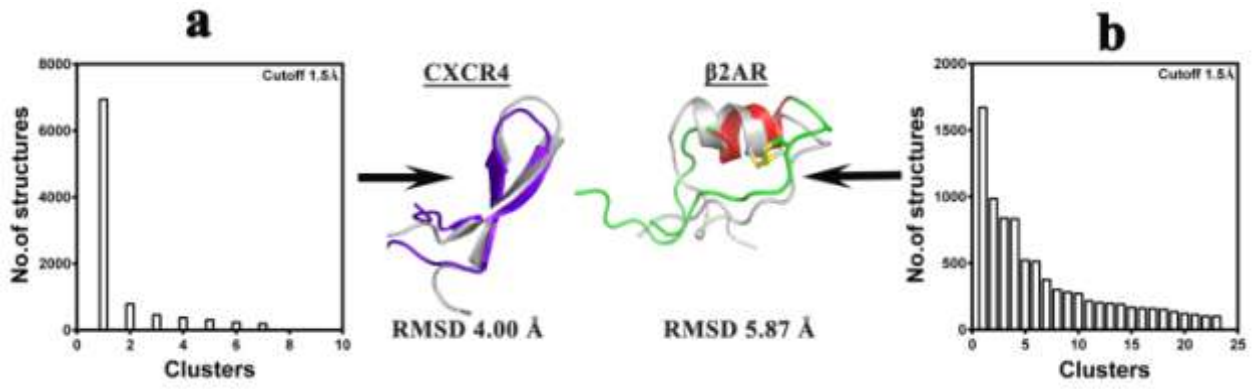

Fig. S5. Superposition of the respective ECL2s of CXCR4 (a, backbone RMSD ~ 4 Å) and β2AR (b, backbone RMSD ~ 5.87 Å) as observed in crystals (gray) against the central conformer of the cluster 1 (major microstate) evolved over 50 ns of MD at 300K. Only the major clusters / microstates are plotted.

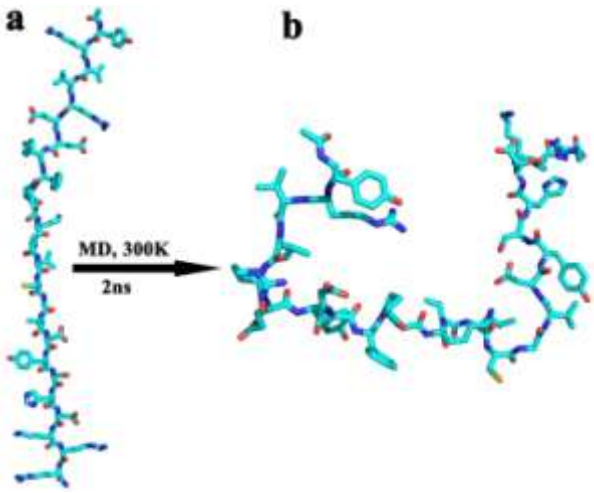

Fig. S6. (a) The extended ECL2 polypeptide of C5aR. (b) The random collapsed conformation of the ECL2 after 2ns of folding simulation in explicit water at 300K.

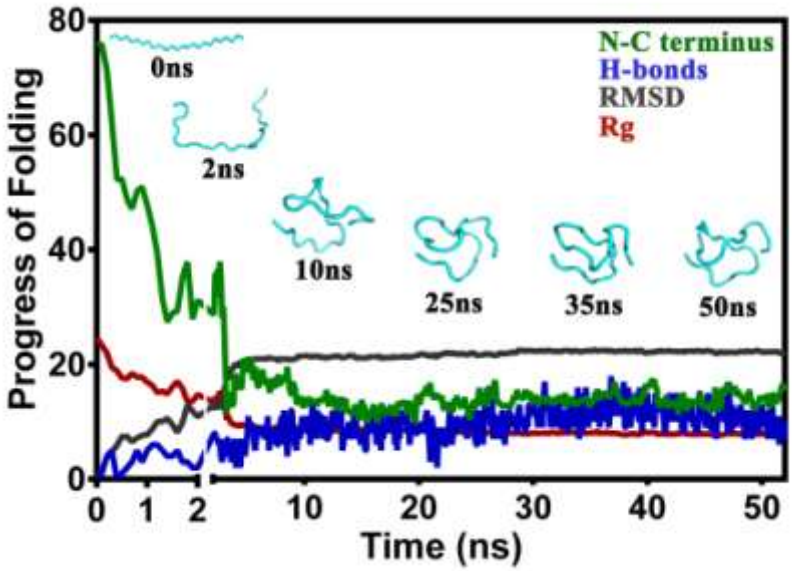

Fig. S7. Monitoring the progress of folding for the C5aR extended ECL2 polypeptide over 50 ns of MD at 300K in explicit water. Formation of molten globule like structures are noted around 25 ns.

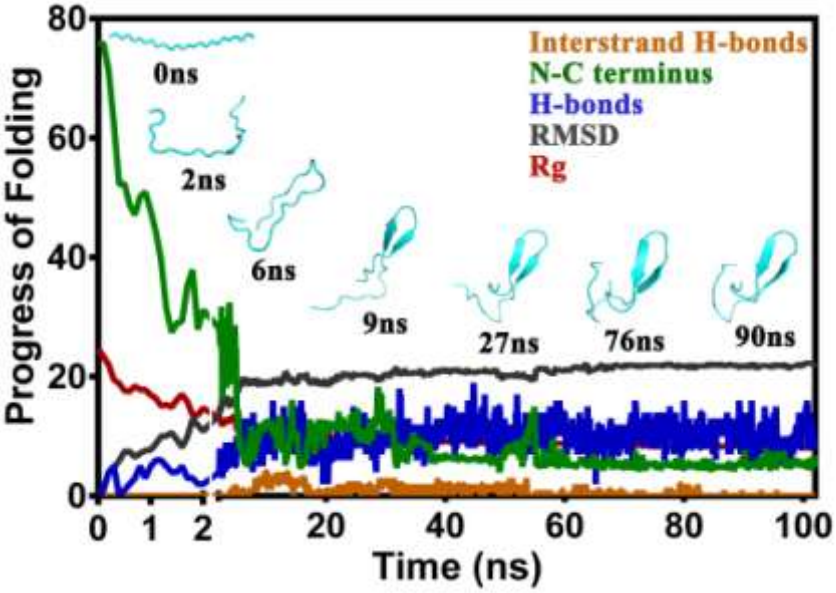

Fig. S8. Monitoring the folding (repeat) of the extended ECL2 polypeptide of C5aR over 100 ns of MD at 310K in explicit water. Folding parameters are highlighted. Nucleation of the β-hairpin like structure is noted at around 6 ns, which remains stable over 100 ns.

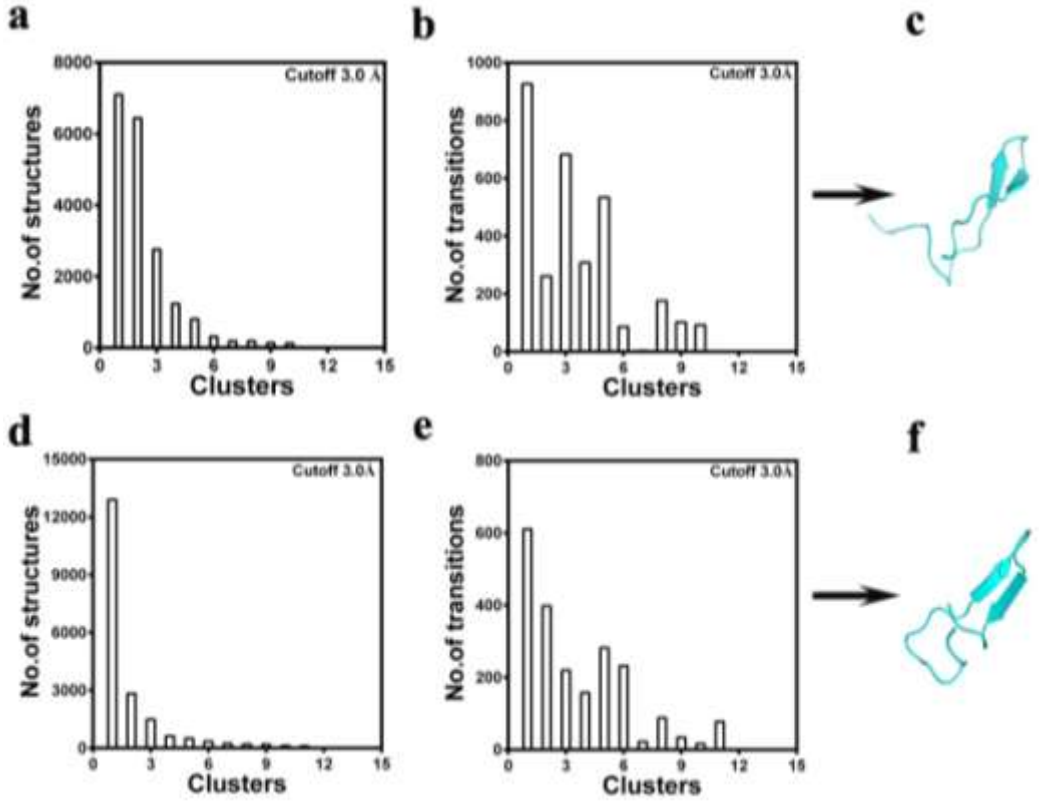

Fig. S9. Cluster analysis of the 310K folding trajectories, respectively displaying the major microstates / clusters and the conformational transition between them (a, b: trajectory 1; d, e: trajectory 2). The representative conformers from the microstate 1 / cluster1 are respectively presented for the trajectory 1 (c) and for the trajectory 2 (f).

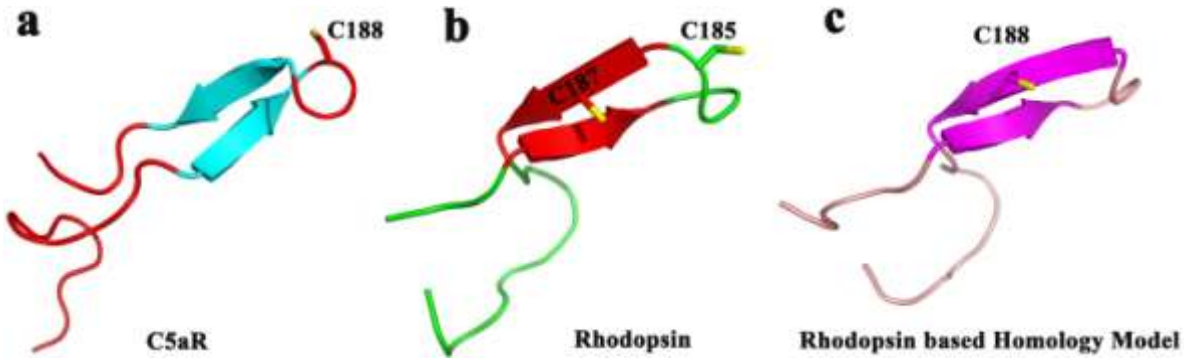

Fig. S10. (a) The ECL2 of C5aR. (b) The ECL2 of rhodopsin sharing a backbone RMSD ~ 6.8 Å with the folded ECL2 of C5aR. (c) The ECL2 observed in the rhodopsin based homology model of C5aR (3CAP, www.gpcr.org/7tm/) sharing a backbone RMSD ~ 3 Å with the ECL2 of rhodopsin. The additional unpaired C185 observed in the ECL2 of rhodopsin is highlighted in green.

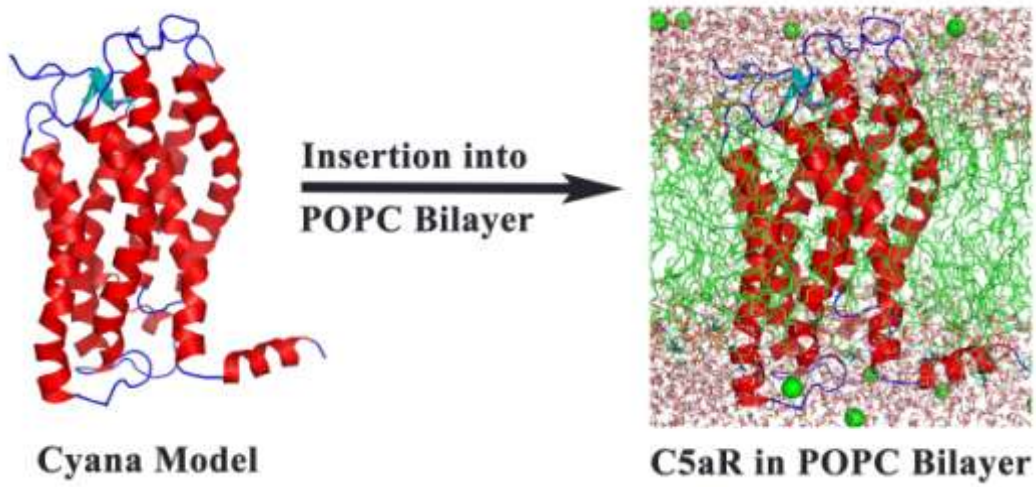

Fig. S11. CYANA modelled C5aR (left) inserted into an equilibrated 1-palmitoyl-2-oleoyl-sn-glycero-3-phosphocholine (POPC) bilayer (right) by recruiting the InflateGRO approach. Figure prepared in PyMOL.

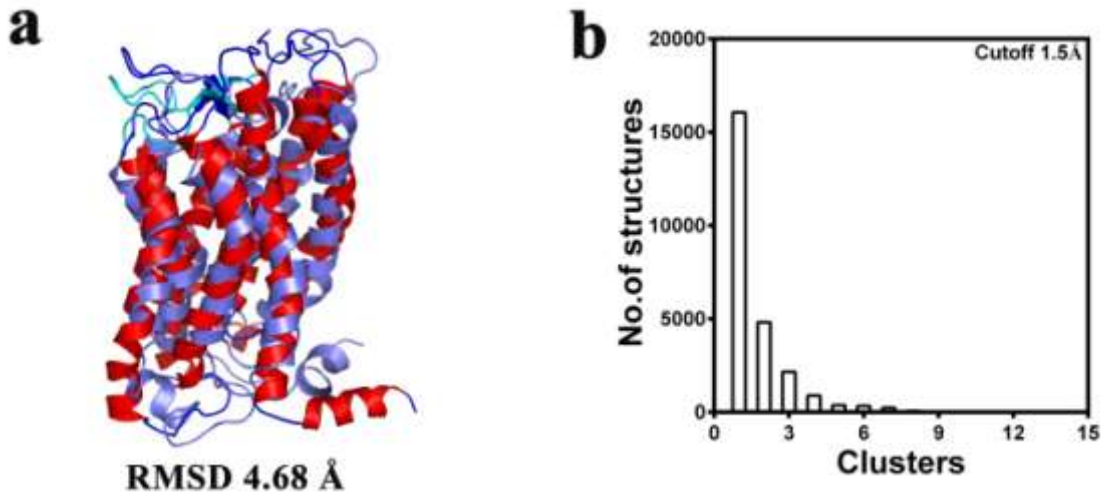

Fig. S12. (a) Superposition of the inactive C5aR (slate) evolved over 250 ns of MD in POPC bilayer at 300K with the CYANA model (red), displaying a backbone RMSD of 4.68 Å. (b) Cluster analysis of the POPC trajectory displaying the number of conformers in each conformational microstate.

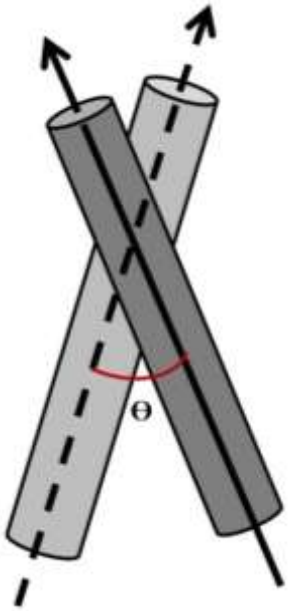

Fig. S13. Schematic illustration of the interhelical angle (Θ) calculated between the helix axes represented in cylinders.

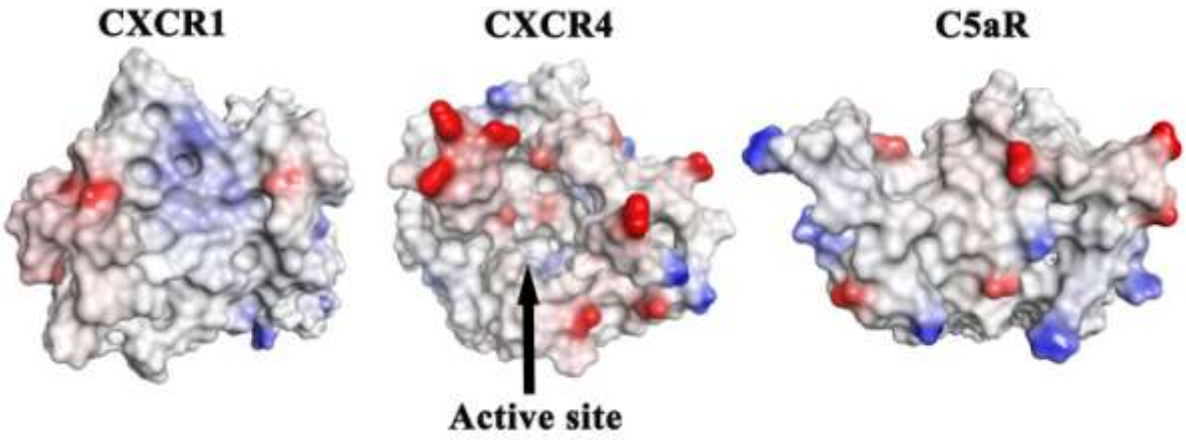

Fig. S14. The contrasting features observed in the ECS of CXCR1 and CXCR4, respectively in the absence and presence of a ligand are compared with the ECS of the inactive C5aR. The receptor surfaces are rendered in ionizability mode and presented at 32° angular perspective. Figure prepared in Discovery Studio.

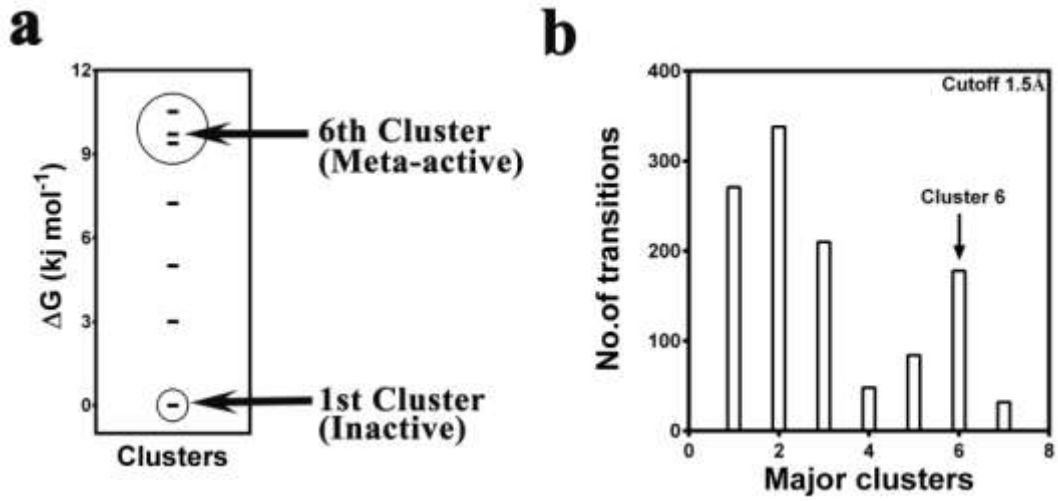

Fig. S15. (a) Energy based ranking of the major clusters highlighting the microstates that provided the inactive (low energy) and meta-active (high energy) conformers of C5aR. (b) Conformational transition observed between the major microstates / clusters. Among the top 3 high energy microstates, the microstate 6 (cluster 6) displaying the highest number of conformational transitions is also highlighted.

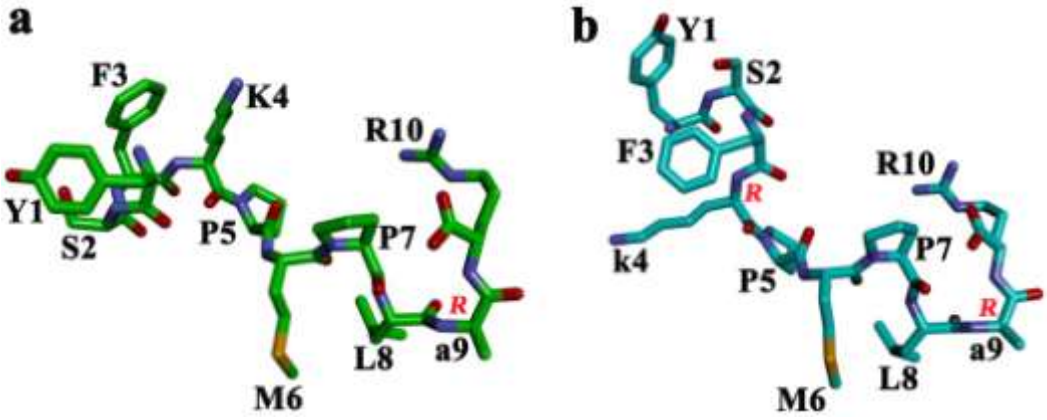

Fig. S16. (a) Energy minimized model of the YSFKPMPLaR agonist and (b) the stereochemical mutant peptide YSFkPMPLaR. The stereochemical centers for the D-amino acids are highlighted in red. The mutant peptide model is based on the NMR structure of the agonist peptide. Figure prepared in Discovery Studio.

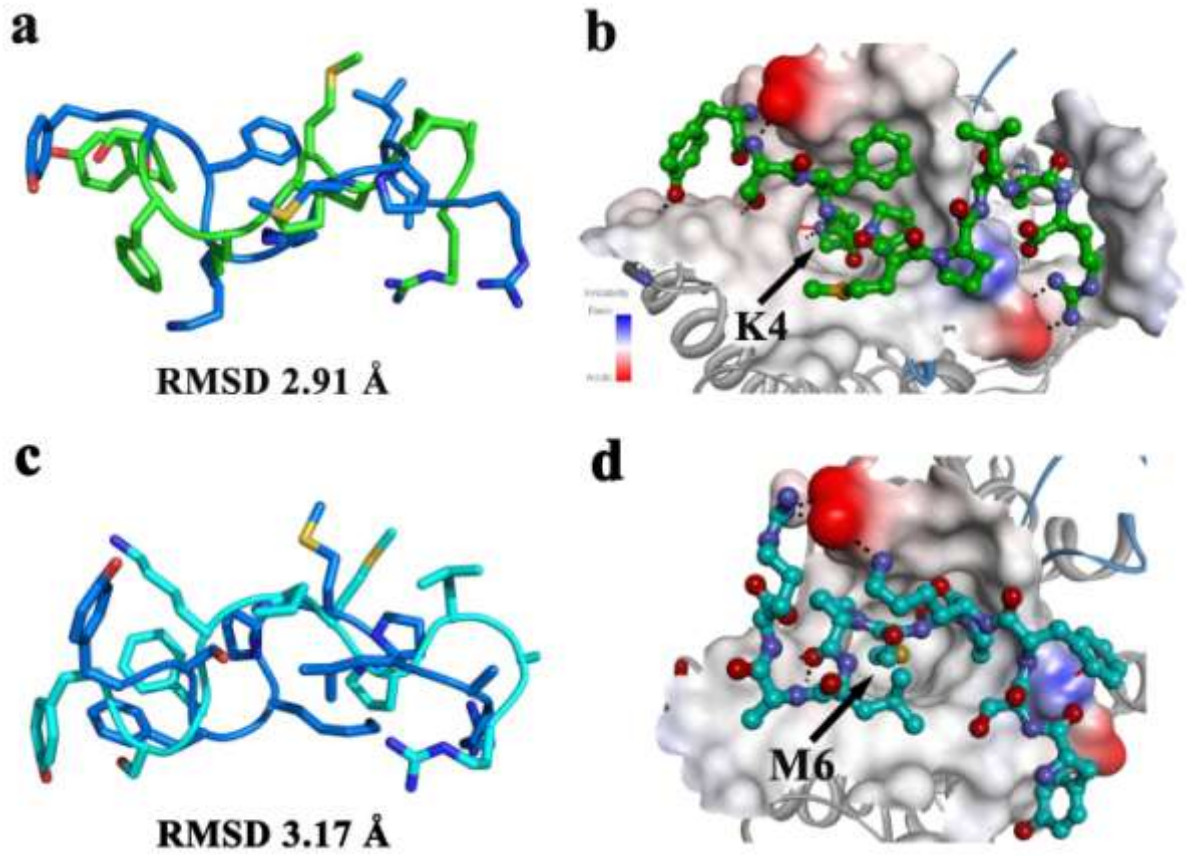

Fig. S17. Change in backbone RMSD of the peptide (blue) post binding to the C5aR in respect to the unbound peptide agonist (a, green) and the mutant peptide (c, cyan). The figures in (b) and (d), respectively highlights the crucial pocket on "site2" occupied by the K4 of the peptide agonist and M6 of the mutant peptide.

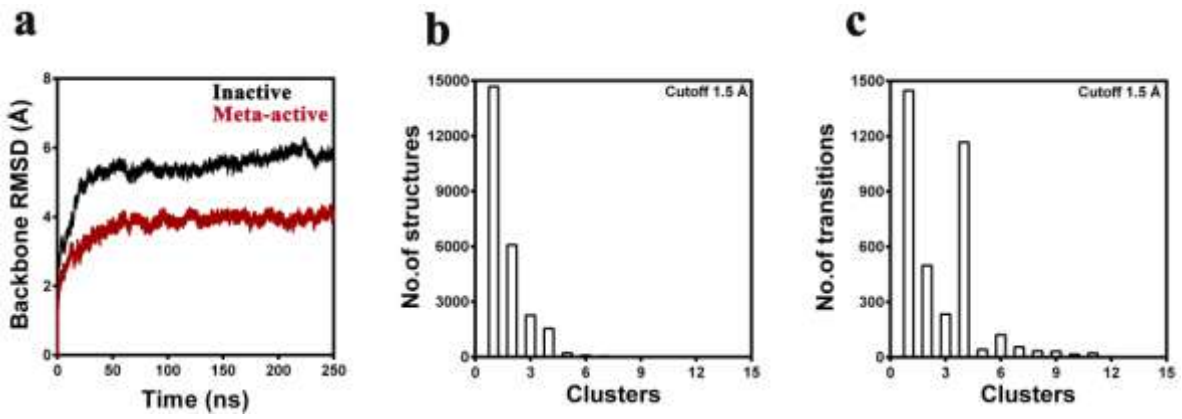

Fig. S18. (a) The backbone RMSD of the inactive and the peptide agonist bound meta-active C5aR plotted over 250 ns of MD at 300K in POPC bilayer. (b) Cluster analysis of the C5aR complex demonstrating the number of conformers in each microstate. (c) Number of conformational transition observed between the major microstates / clusters.

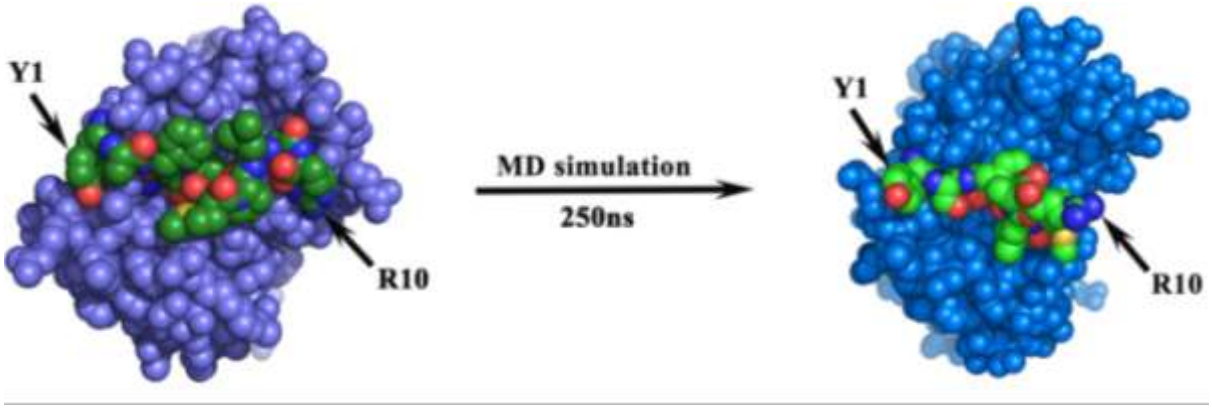

Fig. S19. Overall structural stability of the C5aR complex demonstrated over 250 ns of MD in POPC bilayer at 300K. The left panel illustrates the peptide agonist bound meta-active C5aR prior to the MD simulation. The right panel illustrates the central conformer of the microstate 1 (14675 conformers, Fig. S18b) evolved over 250 ns from the initial C5aR complex (left). The flexibility in R10 side chain of the agonist is highlighted (right) during MD, due to the transient nature of the hydrogen bond interactions with D191 of C5aR.

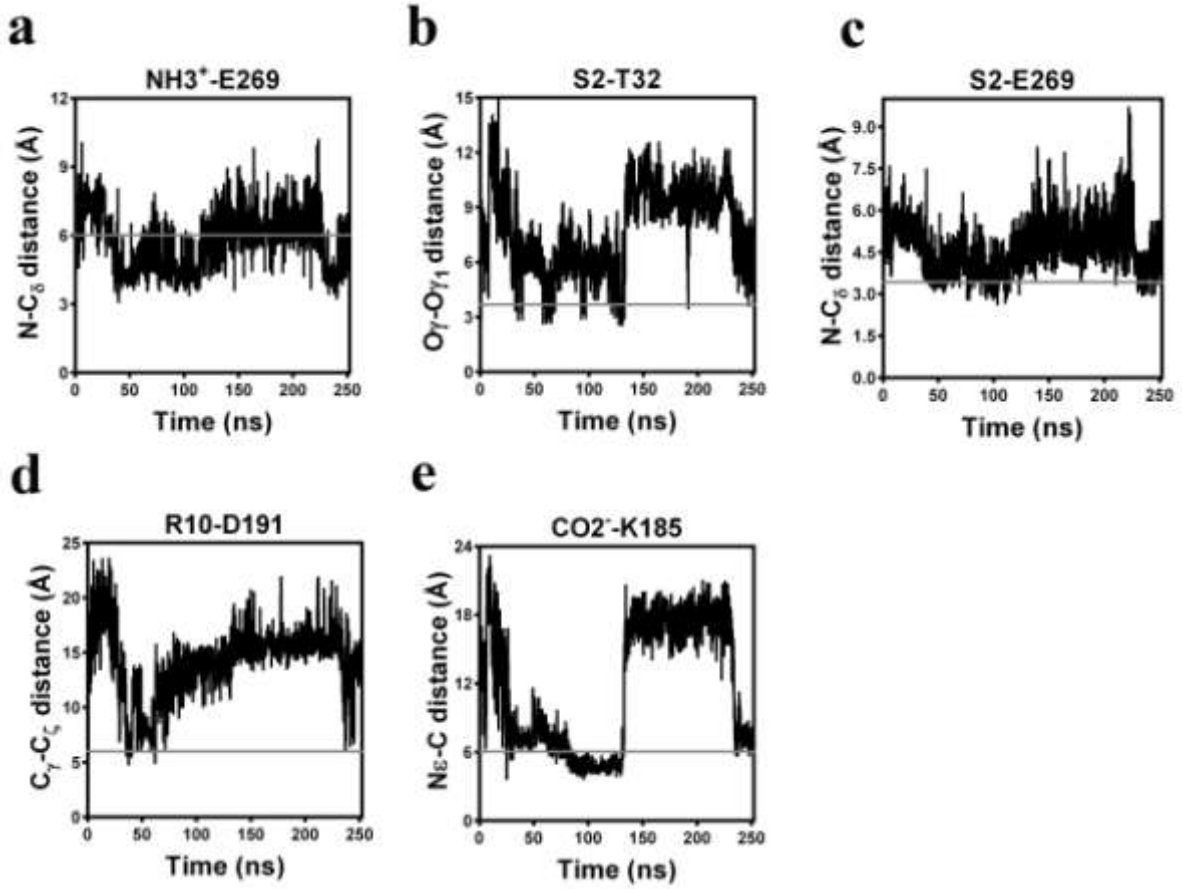

Fig. S20. Monitoring the distance between the heavy atoms involved in the intermolecular interactions, respectively demonstrated in Fig. 7, over 250 ns of MD at 300K in POPC bilayer. The grey solid line indicates the reported cut-off distance

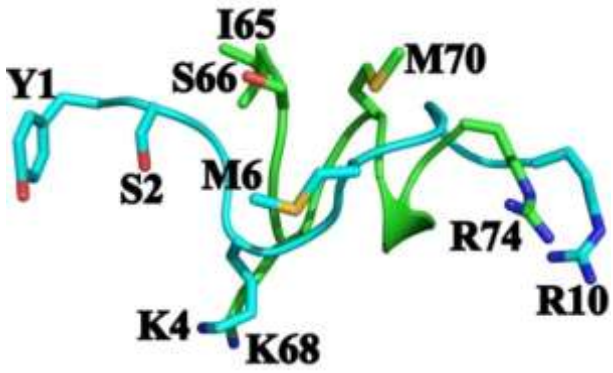

Fig. S21. Conformational similarity observed between the bound conformation of the peptide agonist (cyan) and the unbound conformation of the C-terminus peptide (I65-R74) of C5a (green).